sciendo

POLISH MARITIME RESEARCH 1 (105) 2020 Vol. 27; pp. 180-187
10.2478/pomr-2020-0019

UNDERWATER NAVIGATION SYSTEM BASED ON DOPPLER SHIFT – MEASUREMENTS AND ERROR ESTIMATIONS

Zawisza Ostrowski
Roman Salamon
Iwona Kochańska
Jacek Marszal
Gdańsk University of Technology, Faculty of Electronics, Telecommuniactions and Informatics, Poland

ABSTRACT

A new acoustic navigation system was developed to determine the position and speed of moving underwater objects such as divers and underwater vehicles. The path of an object and its speed were determined by the Doppler shifts of acoustic signals emitted by a transmitter placed on the object and received by four hydrophones installed at the periphery of the monitored body of water. The position and speed measurements were affected by errors mainly caused by acoustic reflections (returns) from the water body boundaries and surface reverberations. This paper discusses the source of the disturbances with the results of a simulation test and experimental measurements. It was demonstrated that the magnitude of the errors could be acceptable in most of the potential applications of the acoustic navigation system.

Keywords: underwater acoustics,navigation systems,Doppler shifts

BACKGROUND

The Doppler effect in hydrolocation systems is usually an undesirable phenomenon and a source of measurement errors [3, 5]. In contrast, the method presented in the article determines the position and speed of moving underwater objects based solely on the Doppler effect [10]. Using this method, the object (a diver or an underwater vehicle) was equipped with a transmitter of a continuous sine-wave sound signal. The transmitted sound signals were received by four hydrophones installed at the periphery of the body of water they were monitoring, and captured and processed by a four-channel receiver. Downstream, the captured digital outputs were further processed by a computer which, at constant time intervals, calculated the Fourier spectra of the received sound signals. The Fourier spectra were used to determine four separate Doppler shift values. The Doppler shift values were accepted as data in a system of non-linear equations, with the unknown values representing the actual position coordinates and coordinate velocity vector components of the object. A method was developed to solve the system of non-linear equations by looking for the solutions at the nodes of a grid which encompassed the monitoring area of the acoustic navigation system. The monitoring area could include shallow bodies of water where underwater search and rescue, monitoring or work could be carried out by human divers and/or autonomous underwater vehicles. The presented method is an alternative solution for classical hydroacoustic navigation systems with a long baseline [6].

The system described below is a simplified version of a system with stationary sound transmitters installed at the periphery of the monitored body of water [4, 7, 8, 9, 11, 12]. The principle of operation of the system was to measure the Doppler shifts of the echo signals created by a moving underwater object.

Similar to every navigation system, it was encumbered by errors of object position and velocity determination. This paper discusses the sources of the errors and characterises their dependency on the system solution and the factors related to sound wave propagation in water.

OPERATING PRINCIPLE OF THE SYSTEM

The system operated in the geometrical arrangement shown in Fig. 1. The transmitter was fixed to a moving underwater object and emitted a continuous sine-wave sound signal at frequency f_0. The sound signal was picked up by four hydrophones installed underwater and outside the monitoring area, the outputs of which were fed to the inputs of a four-channel receiver. The four-channel receiver amplified and filtered the hydrophone outputs, followed by ADC (analogue to digital conversion). The digital outputs of the four-channel receiver were saved to the memory of a PC workstation and processed by discrete Fourier transformation at fixed time intervals, *T*.

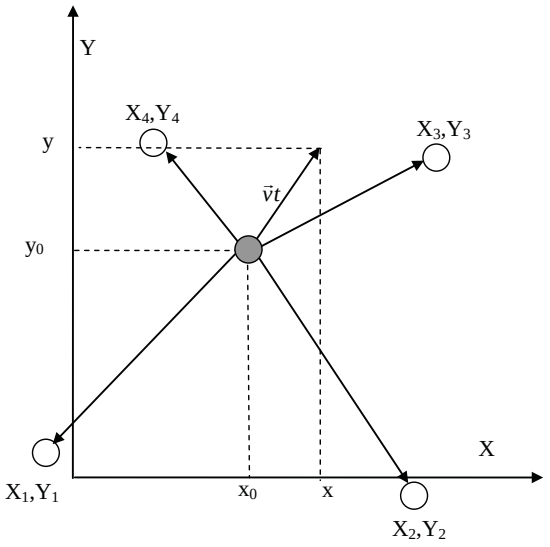

Fig. 1. Geometrical arrangement of the system

The transient spectral frequency was expressed with the following relationship [10]:

$$f_n(t) = f_0 - \frac{f_0}{c}\frac{v_x(x_0-X_n+v_xt)+v_y(y_0-Y_n+v_yt)}{\sqrt{(x_0-X_n+v_xt)^2+(y_0-Y_n+v_yt)^2}} \quad (1)$$

where: c – sound wave speed in water; x_0, y_0 – transmitter position coordinates at time t=0, the start time of each measurement cycle with a duration of T; v_x, v_y – velocity vector components of the object with the transmitter affixed; X_n, Y_n – coordinates of hydrophone number n.

The calculated spectral values were used to determine Doppler shifts, $F_n(t)$, with each being the following difference: $F_n(t)=f_n(t)-f_0$. Fig. 2 shows examples of the Doppler shift spectra for 3 different directions of the target's movement.

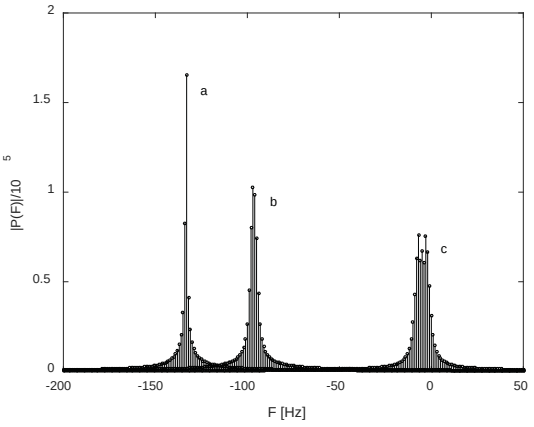

Fig. 2. Doppler shift spectra for 3 different directions of the target's movement

Downstream calculations were based on the Doppler shift values which represented time t=0. These were always the right-hand limit frequencies in the Doppler shift spectrum band, expressed with the following formula [10]:

$$F_n = -\frac{f_0}{c}\frac{v_x(x_0-X_n)+v_y(y_0-Y_n)}{\sqrt{(x_0-X_n)^2+(y_0-Y_n)^2}} \quad (2)$$

Each of the four Doppler shifts (with one per hydrophone) included four unknown values. The unknown values were the initial position coordinates, x_0, y_0, and the velocity vector components, v_x, v_y, of the transmitter. They could be determined as the solutions of a quadruple equation system, in which four Doppler shift values are known for the sound signals picked up by the four hydrophones. Since Eq. (2) had non-linear equations, a method was proposed to solve the equations at the nodes of the grid which encompassed the monitored area. By designating the coordinates of grid node k as x_k, y_k and introducing the following designations,

$$g_n = -F_n\frac{c}{f_0} \qquad x_n = x_k - X_n \qquad y_n = y_k - Y_n \quad (3)$$

Eq. (2) provided the following:

$$g_n = \frac{v_xx_k+v_yy_k}{\sqrt{x_k^2+y_k^2}} \quad (4)$$

The designations

$$a_n = \frac{x_k}{\sqrt{x_k^2+y_k^2}} \qquad b_n = \frac{y_k}{\sqrt{x_k^2+y_k^2}} \tag{5}$$

provided this:

$$g_n = v_x a_n + v_y b_n \tag{6}$$

A system of linear equations as follows:

$$\begin{bmatrix} g_1 \\ g_2 \end{bmatrix} = \begin{bmatrix} a_1 & b_1 \\ a_2 & b_2 \end{bmatrix} \begin{bmatrix} v_x \\ v_y \end{bmatrix} \tag{7}$$

allowed a determination of object velocity vector components v_x, v_y, at every node of the grid. Node grid coordinates x_k, y_k, at which three equations of the following type are fulfilled:

$$\begin{bmatrix} a_1 & b_1 \\ a_2 & b_2 \end{bmatrix}^{-1} \begin{bmatrix} g_1 \\ g_2 \end{bmatrix} = \begin{bmatrix} a_3 & b_3 \\ a_4 & b_4 \end{bmatrix}^{-1} \begin{bmatrix} g_3 \\ g_4 \end{bmatrix} \tag{8}$$

were adopted as the approximate position coordinates of the transmitter: $x_0 = x_k$, $y_0 = y_k$.

Fig. 3 shows examples of locations with the solutions of equation systems (7) and (8) and their common solution, designated with a red circle, which was the transient position of the transmitter. Fig. 4 shows an example of the path of a transmitter determined with the foregoing method. The initial coordinates of the path were designated x_0, y_0, the path inclination angle was designated β, and the transmitter velocity was designated v. The red circles represent the assumed transmitter path and the black stars represent the determined transmitter path.

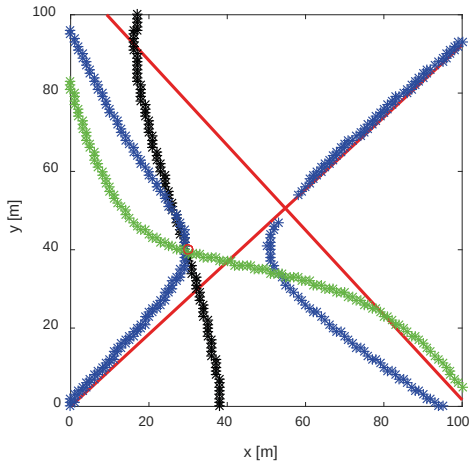

Fig. 3. Geometric locations of the solutions for Eq. (7)

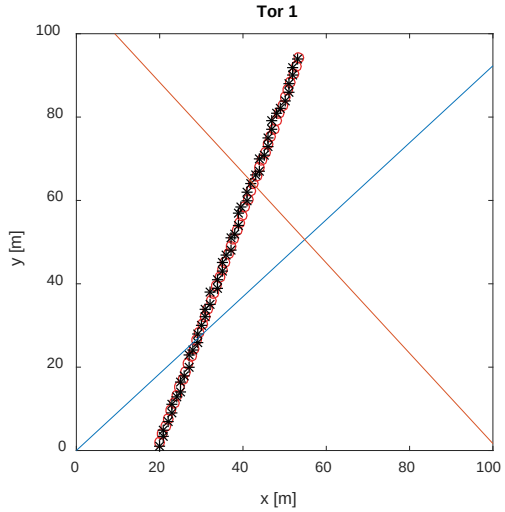

Fig. 4. Path of a straight-line uniform motion (x_0=20 m, y_0=2 m, $|v|$=2 m/s, β=70°)

SYSTEM ERRORS

According to the operating principle of the system explained above, three types of system errors were present in the determination of the transmitter position and velocity. The first system error type was a result of the determination of the transmitter position and velocity at the grid nodes. When the system worked without any malfunction, this first system error type depended on the grid mesh size. When the transmitter position was determined at the nearest node of a grid with a mesh side length of 1 m, the RMS error value, expressed as the deviation from the actual position, was 38.4 cm; it was deemed virtually irrelevant.

The second system error type was a result of the Doppler shift spectrum resolution, a parameter governed by interval T, in which the spectra were calculated. If, for example, T=1s, the frequency measurement resolution would be $\Delta f = 1/T = 1$Hz. By increasing interval T, the Doppler shift measurement resolution was improved at the cost of reduced measurement resolution of the monitored object path.

Fig. 5(a) shows errors Δd of the transmitter position determination with the Doppler shifts calculated at an accuracy achievable in MATLAB® calculations. Fig. 5(b) shows the same errors with the Doppler shift values rounded to the nearest 1 Hz. The examples in the figures are shown for a straight-line uniform motion at velocity $|\vec{v}|$= 2 m/s.

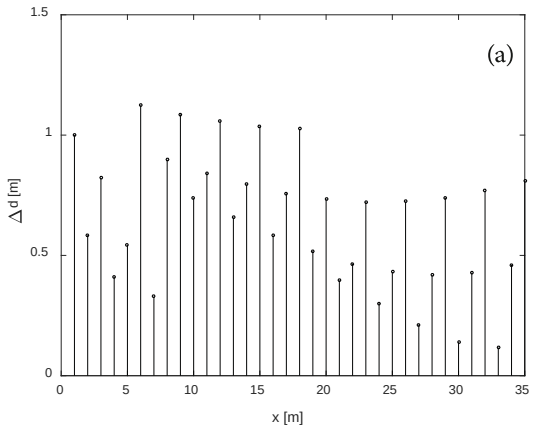

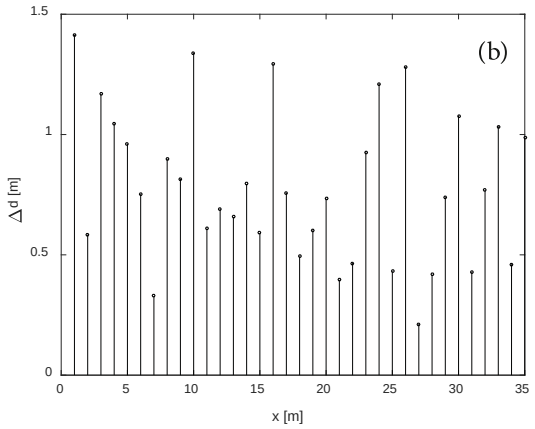

Fig. 5. Transmitter position measurement errors: (a) with accurate values of Doppler shift; (b) with Doppler shift values rounded to the nearest 1 Hz

In this example, the mean position measurement error with accurate Doppler shift values was 0.65 m and with the Doppler shift values rounded to the nearest 1 Hz, it was 0.78 m. The standard deviations were 0.27 m and 0.32 m, respectively. These examples and a series of similar simulations revealed that rounding the Doppler shifts to the nearest 1 Hz did not cause any errors that would reduce the system's performance.

The same conclusions were drawn from the simulations of transmitter velocity determination, the errors of which are shown in Fig. 6, with the path shown in Fig. 5.

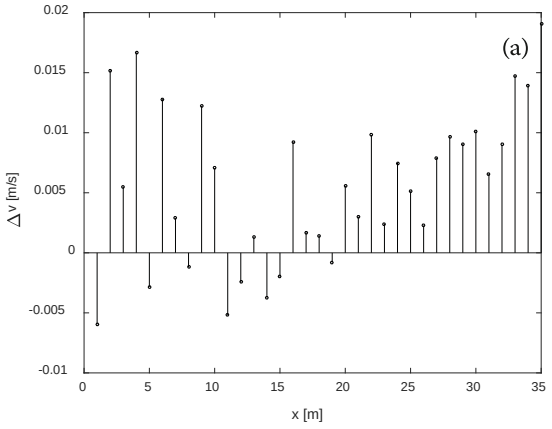

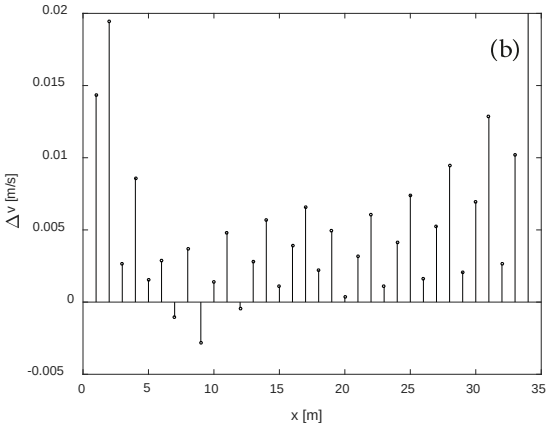

Fig. 6. Transmitter velocity measurement errors: (a) with accurate values of Doppler shift; (b) with Doppler shift values rounded to the nearest 1 Hz

The average velocity measurement error with accurate values of Doppler shift was 5.2 mm/s, and with the Doppler shift values rounded to the nearest 1 Hz, it was 5.6 mm/s. The standard deviations were 5.3 mm/s and 6.5 mm/s, respectively.

The third system error type which manifested itself at specific inclinations of the transmitter path was the determination of two paths, one of which was true. This was an effect of the ambiguity inherent in the Doppler effect, by which one Doppler shift value corresponded to two positions of the transmitter. The false path of the transmitter featured specific characteristics which usually permit its elimination.

EFFECT OF DOPPLER SHIFT MEASUREMENT ERRORS ON THE SYSTEM PERFORMANCE

Acoustic noise, reverberation and wave reflections at the periphery of the body of water could distort the spectra of the sound signals picked up, resulting in erroneous determination of the Doppler shift values. Moreover, to apply the discrete Fourier transformation to the Doppler shift calculation, the measured signal should be wide-sense stationary [1, 2]. A wave on the water surface, internal waves or the movement of the object from which the signal is reflected may cause the first and second order statistical properties of the received signal not to be stationary. In this case, interpretation of the discrete Fourier transform result can be misleading.

To find the relationship between the errors, simulation tests were carried out during which random changes were made to the Doppler shift frequencies determined with theoretical dependencies. It was assumed that the Doppler shift frequencies had a Gaussian distribution with a specific standard deviation σ, and a mean value equal to the theoretical Doppler shift. The frequency measurement resolution of 1 Hz was maintained. The following demonstrates the results of a simulation with straight-line uniform motion. The erroneous frequency shift values were input separately to each of the 10,000 monitoring steps. The probability density distribution for Doppler shift errors δf is shown in Fig. 7. Fig. 8 shows an

example of the effects the errors had on the determination of the transmitter path.

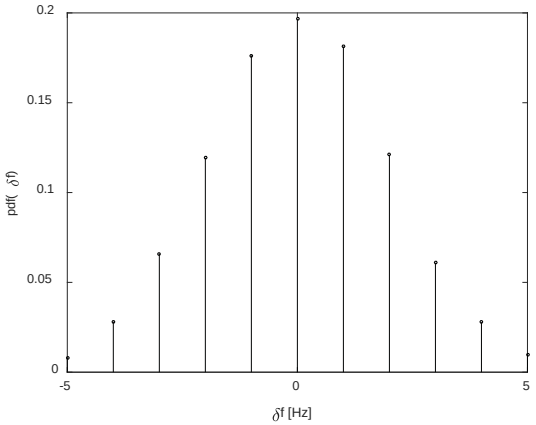

Fig. 7. Probability density distribution

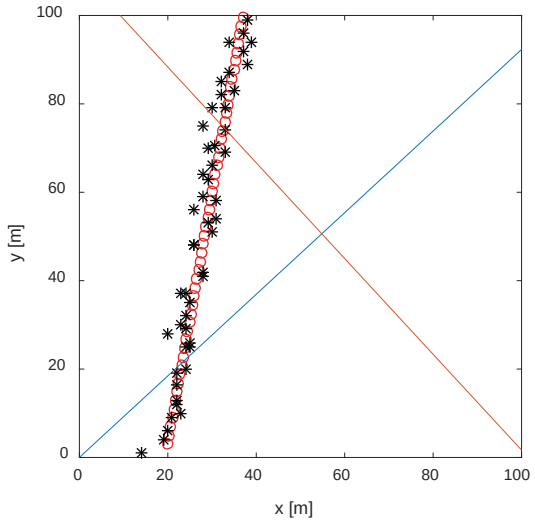

Fig. 8. Transmitter path at for Doppler shift errors (σ = 2 m/s) (σ = 2 m/s, β = 81°, v= 2 m/s)

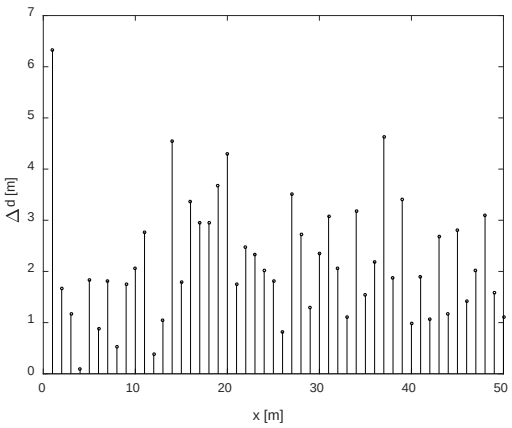

Fig. 9. Transmitter position measurement errors

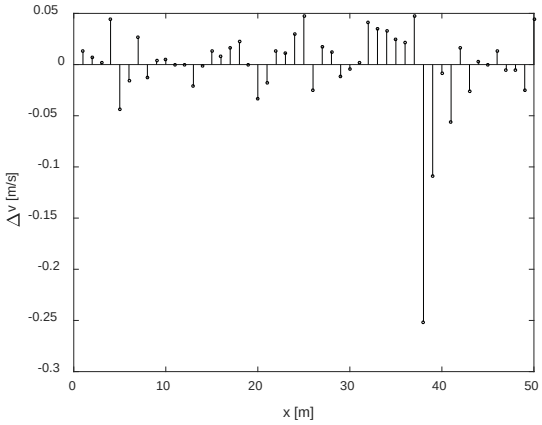

Fig. 10. Transmitter velocity measurement errors

For the observation depicted in Fig. 8, the transmitter position measurement errors are shown in Fig. 9, and the transmitter velocity measurement errors are shown in Fig. 10.

To test the effect of the magnitude of Doppler shift errors on the determination of the transmitter position and velocity, a series of simulations were done with various standard deviation values assumed for Doppler shift errors and various transmitter velocity values. The simulation test results are shown in Table 1.

Tab. 1. Statistical parameters of transmitter position measurement errors ($\overline{\Delta d}$ [m] – mean; σ_d [m] – standard deviation; σ [Hz] – Doppler shift measurement error)

σ [Hz]	$\lvert v\rvert$=1 m/s		$\lvert v\rvert$=2 m/s		$\lvert v\rvert$=3 m/s	
	$\overline{\Delta d}$	σ_d	$\overline{\Delta d}$	σ_d	$\overline{\Delta d}$	σ_d
0.5	1.4	0.8	0.8	0.4	0.8	0.4
1	2.1	1.2	1.2	0.7	1.0	0.4
2	4.0	2.5	2.2	1.2	1.5	0.9
3	6.0	3.6	3.1	1.9	2.1	1.6

The tabulated values suggest that an increase in the standard deviation of the Doppler shift measurement error always caused an increase in the mean value and standard deviation of the transmitter position determination error; the errors grew as the transmitter velocity was reduced. To ensure that the transmitter position determination error was acceptable, a signal-to-noise ratio value at the receiver input was required at which the Doppler shift measurement errors were small.

Parallel testing of the transmitter velocity measurement errors proved that their mean values and standard deviation were extremely low and had no clear trend as a function of the standard deviation of Doppler shift or velocity.

Simulation tests were performed according to the scenario explained below to determine the relationships between the receiver input signal-to-noise ratio and the Doppler shift measurement errors critical to the transmitter position and velocity errors. The transmitter was moving at a velocity of $|v|$=2 m/s (and where the direction of motion was irrelevant) from position x_0=100 m, y_0=100 m, with a hydrophone located at the origin of the coordinate system. The position corresponded to the maximum transmitter-to-hydrophone distance within the

system at which the signal-to-noise ratio was at its minimum. At the same time, the picked-up sound signal spectrum featured only one large line. The transmitter output a sine-wave sound signal at a frequency of f_o = 100 kHz. The receiver input accepting the hydrophone output had a narrow-band filter with a mid frequency of f_o and a frequency response of B=810 Hz, which corresponded to the assumed maximum Doppler shift. The correct detection criterion was assumed to be met when the maximum-height line had a true Doppler shift with a tolerance of ± 2 Hz, approximately equal to σ=2 Hz.

The Doppler shift spectrum was calculated from a signal being the total of the picked-up sine-wave sound signal and white noise at a standard deviation of σ_s. Calculations were carried out in parallel to the simulation tests by applying a periodogram (the square of the determined spectrum modulus). In one thousand iterations of the tested processes, Doppler shift values were determined with their deviations from the true Doppler shift. Once one thousand iterations were completed, a histogram of the errors was developed. The probability of sound signal detection was calculated from five histogram lines between -2 Hz and 2 Hz.

The following figures illustrate the successive steps of the calculations for the pick-up probability determined with the periodogram. Fig. 11 shows the picked-up signal periodogram. The input signal-to-noise ratio was -15 dB with the true Doppler shift at 94 Hz. Fig. 12 shows the Doppler shift errors, dF, present in 1000 measurement iterations.

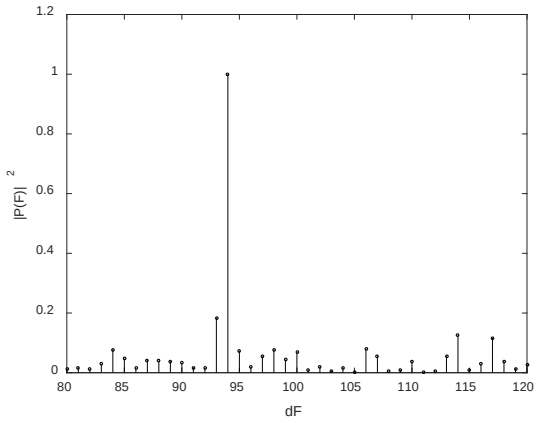

Fig. 11. Doppler shift periodogram

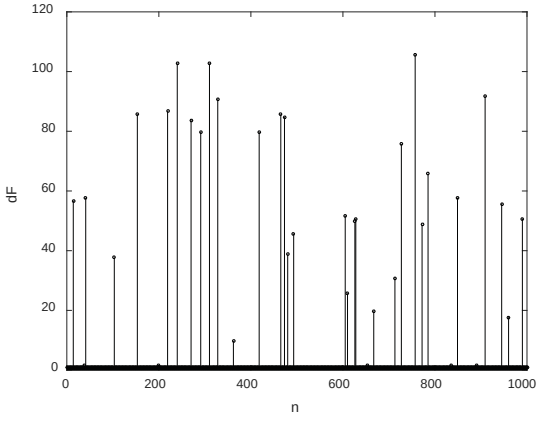

Fig. 12. Doppler shift errors

Once the magnitude and count of the errors were known, a histogram was plotted to determine the probability distribution of the Doppler shift errors, as shown in Fig. 13. The height of each line corresponded to the probability of its detection. The maximum probability was at dF = 1 Hz, which was caused by the rounding applied.

Similar calculations were performed at various input signal-to-noise ratio values, with the results shown in Fig. 14. The red line was the probability determined from the periodogram. The blue line was the probability determined from the picked-up signal spectral modulus. It is evident that the periodogram was more favourable for the application.

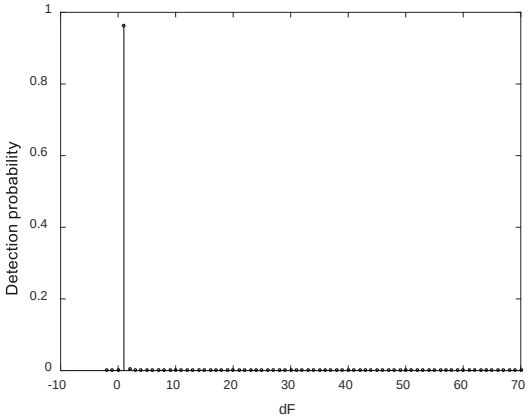

Fig. 13. Detection probability of Doppler shift dF

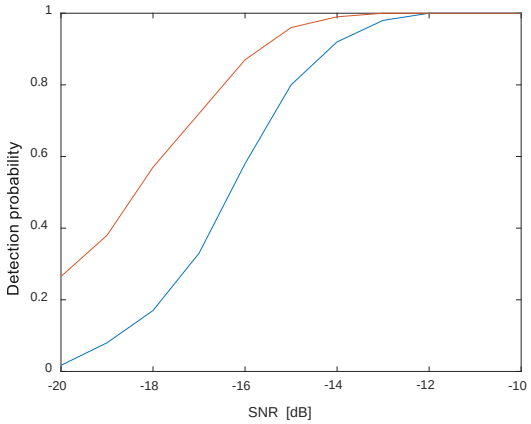

Fig. 14. Probability of correct detection

The chart shown in Fig. 14 revealed that the system could function with the acceptable errors of the determined transmitter position already at negative values of the input signal-to-noise ratio. Example: with the periodogram used, the signal-to-noise ratio of -14 dB gave a detection probability of PD= 0.99. This meant that the Doppler shift measurement error exceeded ± 2 Hz every 100 s on average. Given that the transmitter velocity assumed for the calculations was 2 m/s, the transmitter covered a distance of 200 m in the meantime. The distance was longer than the assumed system range.

MEASUREMENTS OF THE EXPERIMENTAL MODEL

To provide an experimental verification of the computer simulation tests, a model of the system was built and measured in Lake Wdzydze. The transmitter was installed on a motor boat, the position of which was monitored by GPS. Four hydrophones were placed 2 m underwater and outside the monitored water body area of 50×50 m. Examples of the measurement results are shown in Figs. 15 to 18. The red lines denote the transmitter path monitored by GPS. The stars denote the transient positions of the transmitter measured by the system model. The right-hand figures show the transmitter velocity components. The subscripts read the average velocity of the motor boat.

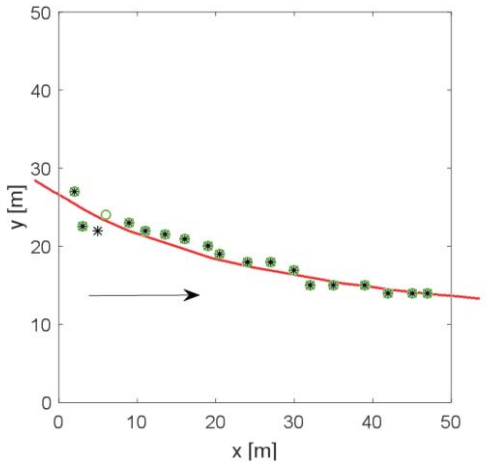

Fig. 15. Transmitter motion path (f_0= 81 kHz)

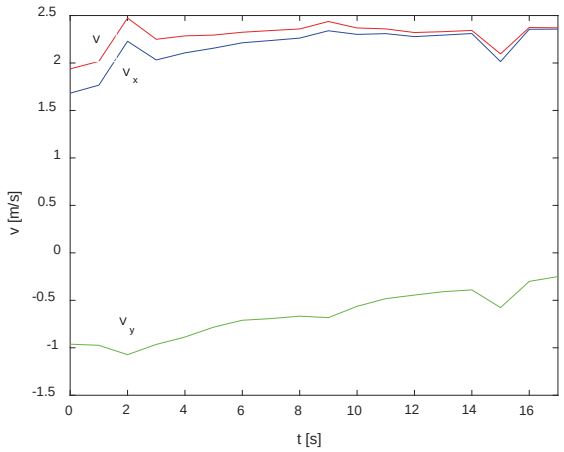

Fig. 16. Transmitter velocity components (v=2.3 m/s)

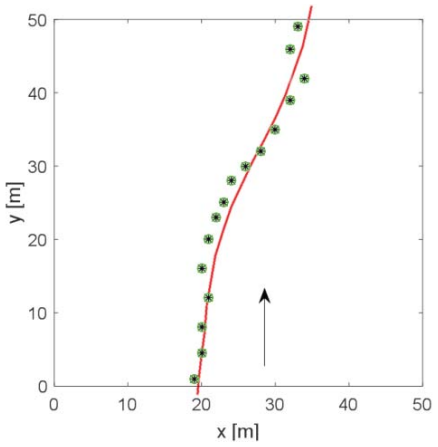

Fig. 17. Transmitter motion path (f_0= 81 kHz)

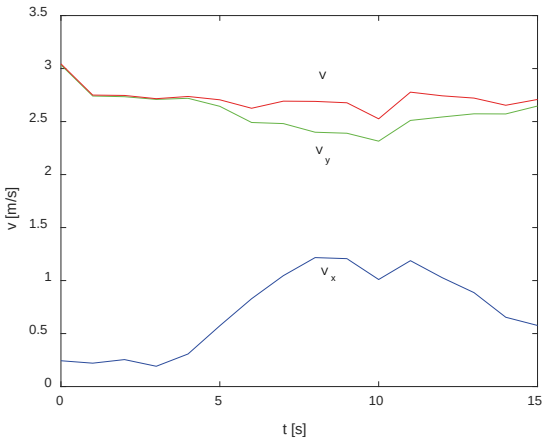

Fig. 18. Transmitter velocity components (v=2.7 m/s)

The measurement results provided by the system model and shown in the foregoing figures, as well as the measurement results not shown in this paper, proved that the system performance was generally correct. No quantitative estimation of errors was performed; the transmitter position errors from GPS are comparable to the errors generated by the system.

CONCLUSION

The foregoing simulation test results and the experimental measurement results of the system model proved that it could be useful as a navigation system for divers and underwater vehicles used in ocean engineering and underwater military operations, including protection against sea mines. An advantage of the system was its high resilience to disturbance, as proven by the acceptable negative signal-to-noise ratio values. These negative signal-to-noise ratio values allow a long system range at low transmission power values, which favours miniaturisation of the transmitter hardware.

REFERENCES

1. Kochanska I. (2020): *Assessment of Wide-Sense Stationarity of an Underwater Acoustic Channel Based on a Pseudo-Random Binary Sequence Probe Signal*. Applied Sciences, 10(4), 1221; doi: 10.3390/app10041221.

2. Kochanska I., Nissen I., Marszal J. (2018): *A method for testing the wide-sense stationary uncorrelated scattering assumption fulfillment for an underwater acoustic channel.* Journal of the Acoustical Society of America, 143, EL116; doi: 10.1121/1.5023834.

3. Marszal J. (2014): *Experimental Investigation of Silent Sonar.* Archives of Acoustics, 39(1), 103-115.

4. Marszal J., Salamon R. (2010): *Multistatic Doppler Sonar for Man-Made Lakes and Water-Power Plants Antiterroristic Protection*. Proc. of the 10th European Conference on Underwater Acoustics, Istanbul 2010, pp. 1333-1339.

5. Marszal J., Salamon R. (2012): *Distance Measurement Errors in Silent FM-CW Sonar with Matched Filtering.* Metrology and Measurement Systems, XIX(2) 321-332.

6. Milne P. H. (1983): *Underwater acoustic positioning systems*, Gulf Publishing Company.

7. Ostrowski Z. J. (2014): *The Doppler effect in a bistatic system for determining the position of moving targets.* Hydroacoustics, 17, 225-234.

8. Ostrowski Z. J. (2015): *Receiver of Doppler multistatic system for moving target detection and tracking.* Hydroacoustics, 18, 141-152.

9. Ostrowski Z. J. (2015): *Doppler Multistatic System for Moving Target Detection and Tracking in Water* [in Polish]. In: Progress of Acoustics, ed. K. J. Opieliński, Polish Acoustical Society, Wrocław, pp. 631-642.

10. Ostrowski Z. J., Marszal J., Salamon R. (2018): *Underwater Navigation System Based on Doppler Shifts of a Continuous Wave*. Proc. 2018 Joint Conference – Acoustics, Ustka 2018, IEEE *Xplore* Digital Library, pp. 240-245.

11. Salamon R. (2012): *Doppler effect in hydrolocation systems* [in Polish]. Proc. 59th Open Seminar on Acoustics, Poznań - Boszkowo, pp. 23-28.

12. Salamon R., Marszal J. (2010): *Doppler estimation method for moving target location*. Hydroacoustics, 13, 225-234.

CONTACT WITH THE AUTHORS

Zawisza Ostrowski
e-mail: zawisza.ostrowski@pg.edu.pl
Gdańsk University of Technology, Faculty of Electronics, Telecommuniactions and Informatics,
ul. Gabriela Narutowicza 11/12, 80-233 Gdansk,
Poland

Roman Salamon
e-mail: roman.salamon@pg.edu.pl
Gdańsk University of Technology, Faculty of Electronics, Telecommuniactions and Informatics,
ul. Gabriela Narutowicza 11/12, 80-233 Gdansk,
Poland

Iwona Kochańska
e-mail: iwona.kochanska@pg.edu.pl
Gdańsk University of Technology, Faculty of Electronics, Telecommuniactions and Informatics,
ul. Gabriela Narutowicza 11/12, 80-233 Gdansk,
Poland

Jacek Marszal
e-mail: jacek.marszal@pg.edu.pl
Gdańsk University of Technology, Faculty of Electronics, Telecommuniactions and Informatics,
ul. Gabriela Narutowicza 11/12, 80-233 Gdansk,
Poland